Transient State (TRAST) Spectroscopy and Imaging: Exploiting the Rich Information Source of Fluorophore Dark State Transitions in Biomolecular and Cellular Studies

Jerker Widengren

Contents

Abstract Dark state transitions of fluorophores are central for all forms of fluorescence-based, single-molecule and super-resolution microscopy and spectroscopy. While these transitions typically are a limiting factor in single-molecule studies, they are a prerequisite for all super-resolution imaging techniques. In this chapter, an additional aspect of reversible dark state transitions is highlighted, namely that they can be used to sense a manifold of biomolecular environments, dynamics, and interactions. By Fluorescence Correlation Spectroscopy such transitions can be analyzed in a straightforward manner, but high time-resolution and single-molecule detection (SMD) conditions are required. To overcome these limitations and make monitoring of dark state transitions widely applicable for studies on biological samples, we have developed a technique called transient state (TRAST) imaging. In TRAST, fluorophore dark state transitions are monitored via the time-averaged fluorescence intensity, and how it varies with the modulation of the excitation light. Here, the concept of TRAST is described, and how it can be experimentally realized within different microscope modalities. Lastly, examples of biological applications are given, demonstrating how biologically relevant

J. Widengren
Experimental Biomolecular Physics, Department of Applied Physics, KTH, Royal Institute of Technology, Stockholm, Sweden
e-mail: jwideng@kth.se

R. Šachl, M. Amaro (eds.), *Fluorescence Spectroscopy and Microscopy in Biology*,
Springer Ser Fluoresc (2023) 20: 355–374, https://doi.org/10.1007/4243_2022_26,
Published online: 4 August 2022

environmental and molecular interaction parameters can be monitored in solutions and in live cells, which are difficult, if possible at all, to follow via regular fluorescence readout parameters.

Keywords Biomolecular environments · Fluorescence · Fluorophore · Photophysics · Spectroscopy

1 Introduction

Fluorescence maintains the position as a dominating readout for cellular and biomolecular studies. This has been further strengthened by the remarkable development of fluorescence imaging and spectroscopy methods, offering single-molecule detection (SMD) sensitivity and super-resolution microscopy (SRM) with nanometer-scale imaging resolution (Nobel prize 2014 [1]). Fluorescence-based SRM, SMD, and SMD-based Fluorescence correlation spectroscopy (FCS) methods offer a unique combination of sensitivity, specificity and resolution in time and space, allowing intricate molecular interaction and localization patterns in cells to be resolved [2, 3]. Yet, the development of new fluorescence methods is not exhausted, but still very active (see, e.g., [4–8] for reviews). Interestingly, many of the major bottlenecks, and thereby also the basis for many of the advances, are to be found in the photophysical aspects, rather than on the optics/hardware side [4, 7].

What sensitivity, readout speed and resolution that can be reached in fluorescence-based spectroscopy and microscopy ultimately depend on the ability to detect a high number of fluorescence photons per molecule, in total and per time unit. This makes parameters such as fluorescence quantum yield, q_F, and photobleaching quantum yields, q_B, critical. Moreover, fluorophore blinking, caused by population dynamics of long-lived, non-fluorescent, triplet (T_1), photo-oxidized ($\dot{R}^+$), photo-reduced ($\dot{R}^-$) or photo-isomerized states, is also of central importance to all forms of fluorescence-based SMD and SRM. In SMD studies blinking is an important factor, which can influence the performance in several ways. Transitions to dark, non-fluorescent states can significantly reduce the molecular brightness and signal-to-background conditions and several of these dark states have also been found to be precursor states of permanent photobleaching. In addition, fluorophore dark state transitions can also obscure observations of single-molecule dynamic events of interest, if occurring on similar timescales. While the brightness of fluorescence molecular emitters is an important figure of merit in most SRM techniques, blinking, or the switching of fluorescence emitters on and off, is at the same time also an absolute prerequisite for all forms of SRM [4–7]. Thus, for several reasons, photophysical aspects is and will likely remain a central issue in SMD and SRM research. Also the spectacular, next-generation SRM techniques now entering the stage [9] critically rely on photophysics and properly controlled fluorophore

blinking, and also here play an equally important role as the optics/instrumentation itself [4, 7].

Beyond their relevance for SMD and SRM, an additional, intriguing aspect of fluorophore blinking events is the longer lifetimes of the underlying dark states, ~10^{-6}–10^{-3} s compared to ~10^{-9} s for fluorescence lifetimes. With 10^3 to 10^6 times longer lifetimes and a correspondingly longer time to interact with the immediate environment, these dark states are often highly environment sensitive. Transitions to and from dark long-lived states are thus capable to reflect microenvironments as well as biomolecular dynamics and interactions in a sensitive way. Interestingly, while multi-parameter detection is an attractive strategy, used in a broad range of fluorescence applications in the biomedical field, multi-parameter readouts, including fluorescence blinking, and the whole set of readout parameters coupled to the underlying dark state transitions, have until recently only been considered to a very limited extent. Transitions into more long-lived dark states take place in several different categories of fluorescence emitters, including organic fluorophores, fluorescent proteins, and various kinds of nanoparticles. In this review, we will focus on transitions in organic fluorophore molecules (summarized in Fig. 1), describe how such transitions can be monitored in a broadly applicable manner, and how such monitoring can provide microenvironmental and molecular interaction parameters which are difficult, if at all possible, to retrieve from traditional fluorescence parameters (intensity, lifetime, emission wavelength and polarization/anisotropy).

2 Transient State Monitoring by FCS and Other Methods

Transient absorption spectroscopy (or flash photolysis, FP), invented more than 70 years ago [10], has for many years allowed detailed studies of photo-induced, transient states of fluorophores. Another alternative, restricted to studies of triplet state population dynamics, is to use the triplet state phosphorescence (room temperature phosphorescence, RTP) [11]. A third alternative is FCS. These three categories of methods to analyze transient state dynamics all have their strengths and weaknesses. In transient absorption spectroscopy (FP) the population kinetics of various states are monitored via their absorption by a separate probing beam, following an excitation pulse [12]. However, the absorption spectra of these transient states can often overlap with those of other photo-induced states, making it difficult to separate them from each other [13]. The technique is also relatively technically complicated, is mainly restricted to cuvette experiments, and lacks the sensitivity for measurements at low (<μM) concentrations. Its use for biomolecular studies is thus limited. The emission originating either directly (phosphorescence) or indirectly (delayed fluorescence) from the first excited triplet state offers some attractive features for biomolecular studies [11]. The long decay times make room temperature phosphorescence (RTP) well suited for monitoring of slow rotational motions, e.g., of membrane proteins by luminescence anisotropy [14], and to probe subtle changes in environmental conditions (viscosities, accessibilities of quenchers, polarities,

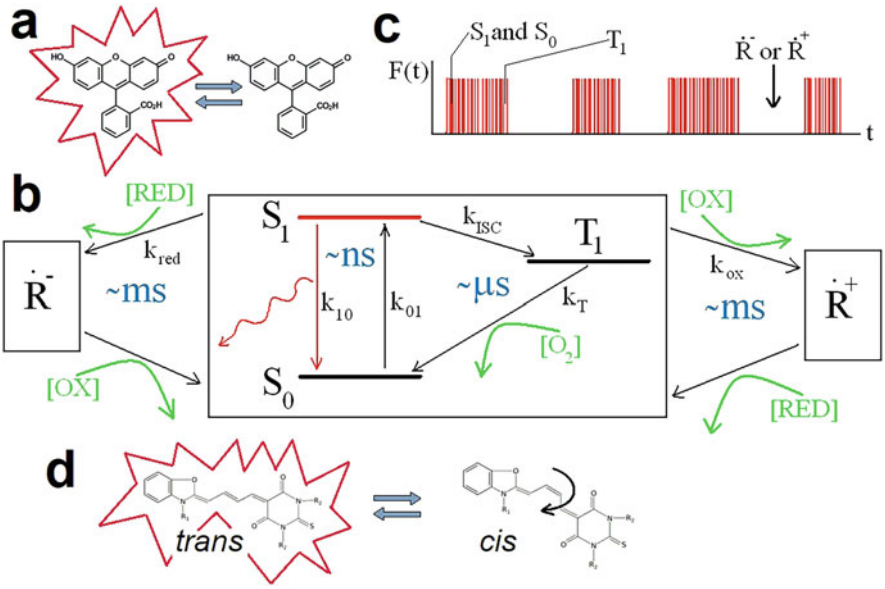

Fig. 1 Common reversible dark state transitions within organic fluorophore molecules. (**a**) Fluorophore blinking follows upon transitions to and from the dark states. (**b**) Representative scheme of underlying states and transitions, where S_0 and S_1 denote singlet ground and first excited states, T_1 the lowest triplet state, and $\dot{R}^+$ and $\dot{R}^-$ photo-oxidized and photo-reduced radical states, respectively. Rates: k_{01} and k_{10} are the excitation and de-excitation rates between S_0 and S_1, k_{ISC} denotes the intersystem crossing rate from S_1 to T_1, and k_T the triplet decay rate back to S_0. Typical timescales of the transitions refer to a typical organic fluorophore in an air-saturated aqueous environment and are indicated in blue. Oxidants [OX], reductants [RED], and molecular oxygen [O_2], as indicated in green, can strongly influence the lifetimes of $\dot{R}^-$, T_1, and $\dot{R}^+$. They can also promote the photo-oxidation and photo-reduction rates (k_{ox} and k_{red}), when present at mM concentrations and higher. With oxidants and reductants present in lower (µM) concentrations, the transitions to and from $\dot{R}^+$ and $\dot{R}^-$ are typically much slower than the transitions between S_0, S_1, and T_1 (within the black box), which then often can be considered as time-averaged on the timescale of the radical state transitions. Fluorescence emission only occurs via excited singlet state decay from S_1 to S_0 (marked red). (**c**) Schematic time trace of the fluorescence from a fluorophore exposed to constant excitation. Short (µs) interruptions are due to transient population of T_1, long ones (ms) to reversible radical state ($\dot{R}^+$ and $\dot{R}^-$) formation. (**d**) Reversible, photo-induced isomerization between a fluorescent, *trans* form and a non-fluorescent, *cis* form of a cyanine dye. The isomerization rates are highly viscosity dependent

etc.), revealing structural and dynamic information of biological macromolecules [15]. However, the RTP signal is weak, and specific RTP probes are scarce and cannot easily be loaded into cells [16]. Coupled to the long-lived RTP emission is also its susceptibility to dynamic quenching by oxygen and trace impurities. Therefore, RTP is largely restricted to deoxygenized, carefully prepared samples, limiting its applications for biomolecular monitoring.

By fluorescence fluctuation analysis with FCS, several of the limitations with FP and RTP readouts can be overcome. In FCS, fluorescence fluctuations are recorded from a sparse number of molecules at a time, passing through a small detection volume, typically comprising a focused laser excitation beam in a confocal arrangement [17] (Fig. 2a). From the recorded fluctuations, as individual fluorescent molecules diffuse into and out of the detection volume, translational diffusion coefficients and absolute concentrations of the fluorescent molecules can be extracted (with knowledge of the dimensions of the FCS detection volume). Similarly, transitions to and from dark states of the fluorescent molecules inside the FCS detection volume can also be determined, from the additional fluorescence fluctuations they generate (Fig. 2b). Taking a simple, standard FCS experiment as an example (Fig. 2a), performed on fluorescent molecules in a solution, which are excited by a focused laser and detected in a confocal arrangement, the total detected fluorescence from the sample volume can be expressed as:

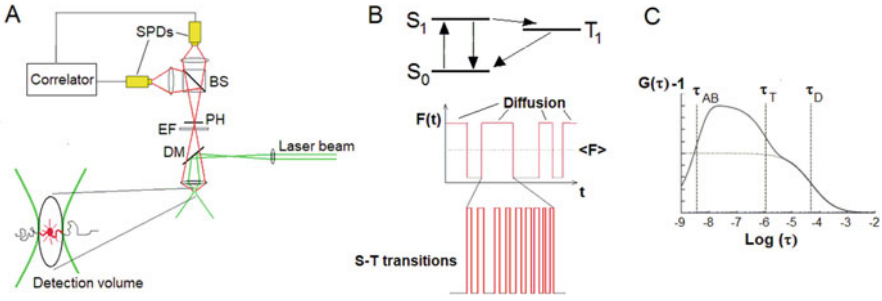

Fig. 2 Measurement of fluorophore dark state transitions by FCS. (**a**) Typical experimental setup for FCS. The beam of a continuous wave (CW) laser is fed into a confocal detection unit. The laser beam is deflected by a dichroic mirror (DM) and then focussed by the microscope objective down to the diffraction limit. The dimensions of the laser beam, together with the collection efficiency function of the microscope define the detection volume (lower left) from which fluorescence is collected. The fluorescence is transmitted through a dichroic mirror (DM), is spectrally and spatially filtered by an emission filter (EM) and a pinhole (PH), located in the image plane. A beam splitter divides the fluorescence into two paths, and fluorescence photons are eventually detected by single-photon counting photodiodes (SPDs). The photocurrents of the SPDs are fed into a PC-based correlator. (**b**) Schematic view of fluctuations in the fluorescence intensity time trace, F(t), as detected by the setup in A from a fluorophore solution, and with the fluorophores freely diffusing into and out of the open confocal detection volume, and undergoing singlet-triplet state transitions on a time scale much faster than the diffusion passage times through the detection volume. (**c**) Calculated FCS curve, given by Eq. (2), showing the time-dependent part of the ACF ($G(\tau)$-1) from a fluorophore undergoing three-dimensional diffusion through an observation volume (Fig. 2a) as well as transitions to and from a non-fluorescent triplet state (Fig. 2b). τ_{AB} and τ_T denote the anti-bunching and the triplet state relaxation times. τ_D refers to the average diffusion time of the fluorophores through the detection volume. The dotted line shows the diffusion-generated part of the FCS curve, denoted $G_D(\tau)$ in Eq. (2)

$$F(t) = q_D \int \mathrm{CEF}(\overline{r}) c F(\overline{r}, t) dV \tag{1}$$

Here, q_D is the detection quantum yield of the instrument, and $\mathrm{CEF}(\overline{r})$ is the collection efficiency function [18]. c is the concentration of fluorescent molecules. Dark state population kinetics of the fluorophores can then be extracted from the fluorescence intensity fluctuations and analyzed in terms of a normalized auto-covariance function, $G(\tau)$, typically referred to as the autocorrelation function (ACF). For fluorophore molecules undergoing diffusion, and in addition also transitions between their ground and first excited singlet states (S_0, S_1) and a dark triplet state (T_1) (Fig. 2b) [19]:

$$\begin{aligned} G(\tau) &= \frac{< F(t)F(t+\tau) >}{< F(t) >^2} \\ &= \frac{1}{N\left(1-\overline{T}\right)} G_D(\tau)\left[1 - \overline{T} + \overline{T}\exp\left(-\tau/\tau_T\right) - \exp\left(-\tau/\tau_{AB}\right)\right] + 1 \end{aligned} \tag{2}$$

Here, square brackets denote time average, N is the average number of fluorescent molecules in the detection volume, $G_D(\tau)$ represents the diffusion-dependent part of $G(\tau)$, and $\overline{T}$ is the average steady-state probability for the fluorescent molecules within the detection volume to be in their triplet states. τ_{AB} and τ_T denote the anti-bunching and the triplet state relaxation times, respectively.

Transient state monitoring by FCS offers a favorable combination of a high signal level (given by the readout of fluorescence photons) and an outstanding environmental sensitivity (given by the long lifetimes of the transient states). It can be realized with a comparatively simple setup, is applicable to a relatively wide range of samples, and can monitor a broad range of fluorescence blinking phenomena, including triplet [19], photo-ionized [20], and photo-isomerized [21, 22] states of fluorophores (Fig. 1). These transient state parameters can provide additional, sensitive information about local oxygen concentrations, redox environments, micro-viscosities, and molecular interactions, which are only very weakly, if at all, reflected in traditional fluorescence parameters (intensity, lifetime, polarization, and wavelength). However, FCS measurements rely on detection of spontaneous fluorescence fluctuations from individual molecules, i.e., SMD conditions are required. This puts high demands on the detection sensitivity and noise suppression. Since the fluctuations of the transient states typically take place in the μs time range, a high time resolution of the detection is also required. Moreover, since low fluorescent signals can typically not be compensated by higher concentrations of fluorescent molecules, FCS measurements rely on a high fluorescence brightness of the investigated molecules [23]. Taken together, FCS measurements put high demands on the detection sensitivity, time resolution, and noise suppression, which limits the applicability of FCS for transient state analyses in biological samples.

3 Transient State (TRAST) Spectroscopy/Imaging: Basic Concept

To overcome the limitations, as encountered in FP, RTP as well as in FCS measurements, our research group has devised a method – transient state (TRAST) monitoring, making transient state measurements more broadly applicable under biologically relevant conditions [24, 25]. The principle of TRAST is illustrated in Fig. 3: The time-averaged fluorescence intensity, $<F>$, from a sample subject to time-modulated excitation is recorded. By systematically varying the excitation modulation, and from how $<F>$ varies with the excitation modulation characteristics, kinetic information about photo-induced, non-fluorescent transient states can be obtained. Like FCS, TRAST combines the detection sensitivity of fluorescence with the environmental sensitivity of long-lived, non-fluorescent states. However, unlike FCS, TRAST is not dependent on the detection of stochastic fluorescence fluctuations from individual molecules. Therefore, TRAST measurements can move away from SMD requirements, and are not limited to the use of fluorophores with high photostability and brightness, nor to samples offering high signal-to-background conditions. The detection quantum yield, q_D, of the instrument is also not critical. Since TRAST also moves the time-resolution requirements from the detection to the excitation side, multi-pixel registration of time-averaged fluorescence can be performed with regular sCMOS and CCD cameras in a parallelized, spatially resolved manner.

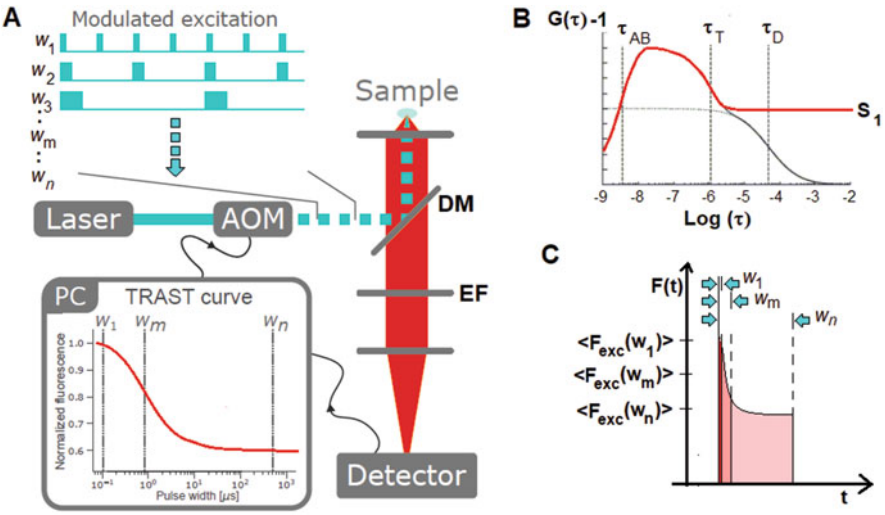

Fig. 3 (**a**) Simplified experimental setup and concept for TRAST. (**b**) Red line: Population probability of the S_1 state, following onset of excitation at time $t = 0$, for a fluorophore undergoing singlet-triplet transitions, as depicted in Fig. 2b. (**c**) Principal drawing of the fluorescence intensity measured in a TRAST experiment for different rectangular excitation pulse durations, w. See main text for further descriptions

For a transient state to be detectable with TRAST, it must be photo-induced and have a different luminescence brightness than the excited singlet state, S_1, within a selected spectral range. Such states are found in most fluorophores, and essentially all long-lived transient states can be considered non-luminescent. Also, the phosphorescence from triplet states is typically negligible, compared to the fluorescence from the S_1 state. Moreover, triplet state phosphorescence is easily quenched and is emitted in a different (longer) wavelength range than the fluorescence. Thus, in most cases, only fluorescence generated upon decay from S_1 to the ground singlet state, S_0 (as depicted in the electronic state model in Fig. 1) needs to be considered. The emitted fluorescence intensity, $F(t)$, will then be proportional to the S_1 population probability, $S_1(t)$:

$$F(t) = k_{10} q_f S_1(t) \tag{3}$$

Here, k_{10} denotes the decay rate from S_1 to S_0, and q_f the fluorescence quantum yield. For a fluorophore subject to constant excitation starting at $t = 0$, $S_1(t)$ can in a general form be described by:

$$S_1(t) = \frac{k_{01}}{k_{01} + k_{10}} \left[1 - e^{-\lambda_{ab} t} - \sum\nolimits_{i=1}^{p} \left[A_i - A_i e^{-\lambda_i t} \right] \right] \tag{4}$$

Here, k_{01} is the excitation rate from S_0 to S_1, given by $\boldsymbol{k_{01} = \sigma \Phi_{exc} = \sigma I_{exc}/h\upsilon}$, with σ denoting the excitation cross-section, Φ_{exc} the excitation photon flux, I_{exc} the excitation intensity and $h\nu$ the excitation photon energy. p denotes the number of different photo-induced non-fluorescent states involved (states other than S_0 and S_1). λ_{ab} and λ_i are the eigenvalues, i.e., the rates of the relaxation modes of $S_1(t)$ upon onset of constant excitation, and A_i the related amplitudes, reflecting the population buildup of the different photo-induced non-fluorescent states. With a suitable initial condition, λ_i and A_i can be described analytically, as functions of the rate parameters in the electronic state model applicable to the fluorophores studied [24]. Assuming that the population of all photo-induced states is zero at $\boldsymbol{t = 0}$, the initial condition becomes $\boldsymbol{S_0(t = 0) = 1}$, i.e., $\boldsymbol{S_1(t = 0) = 0}$. Alternatively, if several states are populated before excitation, the sum of their populations must be 1 at $t = 0$. For most fluorescent molecules, equilibration between S_0 and S_1 after onset of excitation takes place within the time range of the fluorescence lifetime (ns), while the dark state relaxations ($1/\lambda_i$) typically occur on a μs-ms time scale. The S_0-S_1 equilibration time, referred to as the anti-bunching time [26–28] $\boldsymbol{\tau_{ab} = 1/\lambda_{ab}}$, is typically given by [29]:

$$\tau_{ab} = \frac{1}{k_{01} + k_{10}} \tag{5}$$

In TRAST experiments, the modulation of the excitation intensity can in principle be systematically varied in several ways. Typically, square-wave excitation pulse trains are applied, with low duty cycles (1:100 or lower) to avoid dark state

population pile-up effects, and with the time-averaged fluorescence monitored as a function of the duration, w, of the excitation pulses (Fig. 3a). The evolution of $S_1(t)$, or $F(t)$, after onset of a square-wave excitation pulse at $t = 0$ is exemplified in Fig. 3b (red curve), for a fluorophore having three electronic states (S_0, S_1 and T_1), and described by the same state model as in Fig. 2b. Essentially, for a free fluorophore solution subject to a constant I_{exc} in time and space, this curve corresponds to the initial, time-dependent part of the ACF in Fig. 2c, to the part which is not generated by fluorophore diffusion. For a square-wave excitation in a TRAST experiment, and for the ACF recorded in a corresponding FCS measurement with the same constant I_{exc}, the same initial condition applies; Since the ACF reflects the probability to detect a second fluorescence photon from a fluorescent molecule in the sample, given that a first fluorescence photon is detected from it at $\tau = 0$, means that the fluorophore must be in S_0 at $\tau = 0$ (unless there are several independent emitters on the fluorescent molecule). Likewise, before onset of a square-wave excitation pulse in a TRAST experiment, the fluorophore can generally be considered to be in the S_0 state.

In a TRAST experiment, for a sample of fluorescent molecules studied in a confocal setup, subject to a square-wave excitation pulse train with n pulses of duration w and period T, the detected time-averaged fluorescence, $\langle F(w)\rangle$, can then be expressed as [24, 25, 30, 31]:

$$\langle F(w)\rangle = \frac{1}{n \cdot T} \iiint cq_D q_f \mathrm{CEF}(\bar{r}) k_{10} \sum\nolimits_{i=1}^{n} \left(\int_0^w S_{1,i}(\bar{r}, t) dt \right) dV \tag{6}$$

Here $n{\cdot}T$ is the total duration of the excitation pulse train, c the concentration of the fluorescent species, q_D the overall detection quantum yield of the instrument, and CEF the collection efficiency function of the confocal setup. The term $S_{1,i}(\bar{r}, t)$ denotes the probability that a fluorescent molecule, located at $\bar{r}$ in the confocal detection volume, is in its excited singlet state at time t after onset of the i:th excitation pulse, and its time dependence can be described by Eq. (4). Dividing $\langle F(w)\rangle$ with the pulse train duty cycle ($\eta = w/T$) yields the average fluorescence intensity within an excitation pulse:

$$\langle F_{exc}(w)\rangle = \langle F(w)\rangle / \eta \tag{7}$$

$\langle F_{exc}(w)\rangle$ normalized to 1 for pulse durations $|\lambda_{ab}|^{-1} < < w < < |\lambda_i|^{-1}$, denoted $\langle F_{exc}(w)\rangle_{norm}$, represents the averaged population of S_0 and S_1, within the pulse duration, and over the detection volume:

$$\begin{aligned} \langle F_{exc}(w)\rangle_{norm} &= \langle S_0(w) + S_1(w)\rangle \\ &= \frac{\iiint \mathrm{CEF}(\bar{r}) \dfrac{k_{01}(\bar{r}) + k_{10}}{k_{01}(\bar{r})} \left(\dfrac{1}{w} \displaystyle\int_0^w S_{1,i}(\bar{r}, t) dt \right) dV}{\iiint \mathrm{CEF}(\bar{r}) dV} \end{aligned} \tag{8}$$

From Eq. (8), and with knowledge of $I_{\mathrm{exc}}(\overline{r}) = h\nu\Phi_{\mathrm{exc}}(\overline{r})$ yielding $k_{01}(\overline{r}) = \sigma\Phi_{\mathrm{exc}}(\overline{r})$, CEF$(\overline{r})$, and the electronic state model, the transient state rate parameters can then be determined from the pulse duration dependence of $\langle F_{\mathrm{exc}}(w)\rangle_{\mathrm{norm}}$, making up a so-called TRAST-curve [24, 25, 30, 31] (Fig. 3a). Approximating the average excitation rate in the detection volume by:

$$\overline{k}_{01} = \frac{\int k_{01}(\overline{r})\overline{S}_1(\overline{r})\mathrm{CEF}(\overline{r})dV}{\int \overline{S}_1(\overline{r})\mathrm{CEF}(\overline{r})dV}, \tag{9}$$

where $\overline{S}_1(\overline{r}) = k_{01}(\overline{r})/(k_{10} + k_{01}(\overline{r}))$, i.e., the S_1 population at onset of excitation, after equilibration between the singlet states, but before dark state buildup. A simplified expression for $\langle F_{\mathrm{exc}}(w)\rangle$ can be obtained, given by

$$\langle F_{\mathrm{exc}}(w)\rangle_{\mathrm{norm}} = \frac{1}{w}\,\frac{k_{10} + \overline{k}_{01}}{\overline{k}_{01}}\int_0^w S_1(t)dt, \tag{10}$$

with $S_1(t)$ given by Eq. (4), and according to the electronic state model applicable for the particular fluorophores studied.

4 TRAST: Some Experimental Realizations and Applications

Above, we have taken as an example the implementation of TRAST in a confocal setup, where the fluorescence of a sample is induced by a time-modulated stationary laser excitation beam, and the time-averaged fluorescence intensity is detected in a likewise stationary confocal detection volume. As discussed above, the experimental requirements for TRAST are much more relaxed than in FCS. Therefore, the TRAST approach can be made compatible with a range of other modalities for excitation time-modulation, combined with average fluorescence intensity detection. Such modalities include time-modulated wide-field excitation, moving arrays of laser foci or laser excitation fringe patterns, as well as various spatial confinement strategies of the excitation and/or the detection [24, 25, 31]. Apart from realizing TRAST in a stationary confocal microscope arrangement [24, 30, 32], as outlined above, and TRAST implemented with wide-field microscopy (Fig. 4a) [33–35], other experimental setups demonstrated for TRAST include total-internal-reflection microscopy with evanescent-field excitation [36], light-sheet excitation microscopy [37, 38], and two-photon-excitation microscopy [39]. Evidently, the time-modulated excitation experienced by a stationary sample can also be generated by translation of the sample with respect to the excitation, or vice versa. In this way, the excitation need not be idle, and in particular for low duty cycle excitation, a larger sample

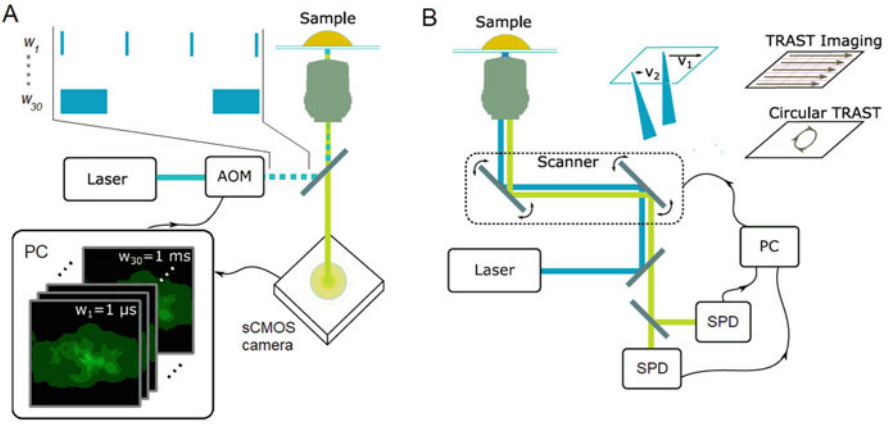

Fig. 4 TRAST imaging implemented with wide-field microscopy (**a**) and confocal laser scanning microscopy (CLSM) (**b**). Blue lines: Excitation laser beam paths, with different scanning speeds applied for CLSM (v_1, v_2, ...) as a means to vary the excitation pulse duration in the different locations in the sample. In the wide-field setup, the excitation light is stationary and modulated in time by an acousto-optical modulator (AOM). Green lines: Paths for the generated fluorescence light

volume can be interrogated within the same period of time. Based on this concept, TRAST imaging can also be well implemented in a confocal laser scanning microscope (CLSM) (Fig. 4b) [31].

Relaxed requirements on noise suppression in the samples, on the fluorescence brightness of the molecules studied, as well as on the detection quantum yield and time-resolution of the instrument, makes TRAST broadly applicable, and it has been demonstrated for studies in solution [24, 31, 36], live cells [33–35, 37] and in bacterial biofilms [38]. Moreover, since high fluorescence brightness is not required, also less bright, auto-fluorescent molecules can be studied [32, 39]. Figures 5 and 6 illustrate different applications of TRAST imaging of live cells, which allow additional microenvironmental information within the cells to be imaged, which are difficult, if possible at all to image via regular fluorescence parameters (intensity, emission wavelength, anisotropy/polarization, fluorescence lifetime). Figure 5a shows wide-field TRAST microscopy images of MCF7 (breast cancer) cells, displaying the triplet decay rates of Eosin fluorophores loaded into the cells [33]. Eosin and most other organic fluorophores undergo intersystem crossing into long-lived, dark triplet states. Triplet states are readily quenched by oxygen, and their lifetimes depend strongly on the local oxygen concentration (~µs in an air-saturated aqueous solutions, ~ms in the absence of oxygen). Triplet state lifetimes of fluorophores thus reflect local oxygen concentrations in a very sensitive manner. By wide-field TRAST imaging of singlet-triplet population kinetics of fluorophores in live cells, it is thus possible to image local oxygen concentrations, and oxygen metabolism, on a sub-cellular level. Figure 5a shows regular fluorescence (middle row) and triplet decay TRAST images (lower row) of MCF7 cells. In

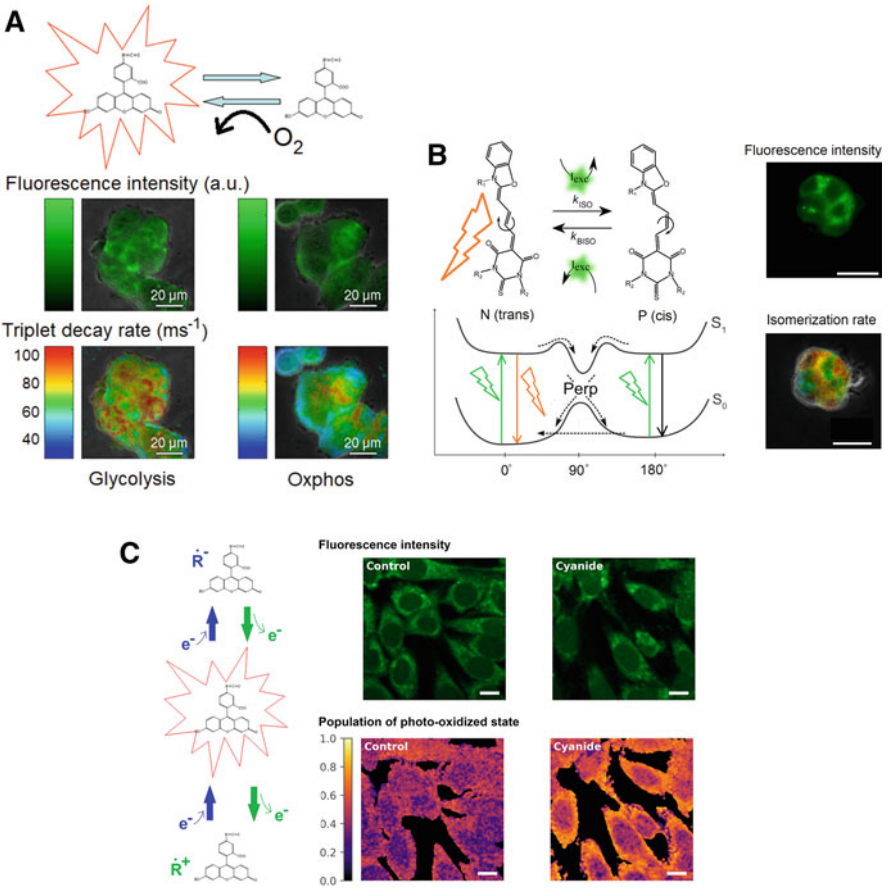

Fig. 5 TRAST imaging of metabolic, redox and microenvironmental conditions in live cells. Triplet state (**a**), photo-isomerization (**b**) and redox-state kinetics (**c**) of added fluorophores (**a** and **b**) or auto-fluorescent NADH (**c**) measured in live cells. (**a**) Regular fluorescence (middle row) and triplet decay TRAST images (lower row) of MCF7 cells, loaded with a high triplet yield fluorophore (Eosin). The triplet decay rate (k_T) of the fluorophore depends almost exclusively, and linearly, on the local oxygen concentration (as depicted in top row). Cells producing ATP primarily by glycolysis (left column), as is often the case for cancer cells, consume less oxygen. Thus, the local oxygen concentration can remain higher, and also the local k_T rates are higher. Cells with normal ATP production via oxidative phosphorylation (right column) consume more oxygen, local oxygen concentrations are lowered, with lower k_T rates as a result. See main text and [33] for further details. (**b**) Left: Excitation-driven isomerization (k_{ISO}) and back-isomerization (k_{BISO}) of a cyanine fluorophore (MC540), leading to transitions between a fluorescent, *trans*, conformation (N) and a non-fluorescent, *cis*, conformation (P). Right: Fluorescence (top) and TRAST (bottom) image of a live cell (MCF7), to which lipophilic MC540 was added and accumulated in the plasma membrane. The TRAST image shows the isomerization rate of MC540 on the cell, which reflects the local fluidity of the plasma membrane. See main text and [34] for further details. (**c**) Label-free TRAST imaging of mouse myoblast cells, using two-photon excitation of the auto-fluorescent co-enzyme NAD(P)H in the cells. In the imaging the excitation pulse duration was varied by the scanning speed of the excitation laser beam over the sample (as in Fig. 4b). Left: Schematic view of photo-induced transitions into transient radical states ($\dot{R}^+$ and $\dot{R}^-$) of a fluorescent molecule. For NAD(P)H, mainly transitions into $\dot{R}^+$ need to be considered. Right: Fluorescence (top row) and TRAST (lower row)

the experiments different growth media were used, so that oxidative phosphorylation (Oxphos) was either ongoing in the cells, or was instead funneled into glycolysis. This metabolic switch away from Oxphos is characteristic for cancer cells (the Warburg effect) and leads to a lower oxygen consumption [41–45]. While no distinction between the two categories of cells was possible to do from the fluorescence images, a higher triplet decay rate (reflecting a higher local oxygen concentration and a lower oxygen consumption) could be seen in the TRAST images taken from cells focused on glycolysis, i.e., TRAST triplet state imaging allows cells with a cancer-specific metabolism to be distinguished from cells undergoing regular metabolism. Figure 5b illustrates how excitation-driven *trans-cis* photoisomerization of cyanine dyes can be imaged by wide-field TRAST, using the same procedure as in Fig. 5a and as described above (Fig. 4a). Trans-cis photoisomerization can be well characterized by FCS (if SMD conditions are at hand) [21, 22] and the isomerization rates are sensitive to several environmental factors, including local viscosity and steric constraints experienced by the fluorophores. More recently, this environmental sensitivity attributed to isomerization of cyanine dyes has been exploited to monitor biomolecular conformations and interactions, where so-called protein-induced, or nucleic acid-induced fluorescence enhancement (PIFE/NAIFE) is detected via FCS, or indirectly via fluorescence intensity and lifetime measurements [46, 47]. Wide-field TRAST imaging allows the isomerization of cyanine dyes to be directly monitored in live cells, on a sub-cellular level. Figure 5b shows TRAST images of the isomerization rates of the lipophilic dye Merocyanine 540 (MC540), reflecting the local viscosity of the cellular membranes [34]. Figure 5c illustrates how TRAST imaging also can monitor photo-induced redox reactions (photo-oxidation or photo-reduction) of fluorescence emitters [39]. These reactions often take place on a somewhat slower timescale than singlet-triplet transitions ([48, 49], see also Fig. 1) and can provide information on the local redox environments of the emitters. The TRAST images in Fig. 5c were recorded by laser scanning microscopy (by the approach shown in Fig. 4b), where the fluorescence of the auto-fluorescent co-enzyme NAD(P)H was recorded upon two-photon excitation and at different scanning speeds of the excitation laser [39]. These images illustrate that TRAST can also be applied on less bright emitters, including auto-fluorescent compounds, and that label-free, live cell TRAST imaging is possible.

As a general remark to the examples in Fig. 5a, c, it can be noted that altered cellular metabolism and redox control are central features underlying development and progression of many diseases, including diabetes, infections, autoimmune diseases and cancer [41–44]. In cellular oncology, reprogramming of energy metabolism is considered a "hallmark of cancer" [50]. Yet, many details remain

Fig. 5 (continued) images, where the color scale of the TRAST images is proportional to the buildup of the $\dot{R}^{+}$ state of NAD(P)H in the cells. The buildup is increased in cells exposed to the mitochondrial blocker cyanide (right column). See main text and [39] for additional details

un-resolved, and the mechanisms are far from understood. In this context, fluorescence blinking parameters, highly sensitive to local cellular oxygen concentrations and redox conditions, can add important information regarding the metabolic and redox status of cells, and can thereby possibly contribute to new diagnostics of different forms of cancer, and other diseases where cellular metabolism and redox control are central.

As a final example, Fig. 6 (right) shows how TRAST imaging can be applied to characterize low-frequency, intermittent interactions between molecules in cellular membranes, by monitoring the quenching of dark transient states of a membrane fluorophore by spin labels in the same membranes. Traditionally, dynamic quenching of fluorescence emission is a widely used approach for biomolecular interaction and conformation studies [51]. In such quenching studies, the fluorescence signal can typically be detected with excellent sensitivity. However, most fluorophores have excited state lifetimes in the range of nanoseconds, whereas bimolecular diffusion-mediated processes in biological membranes typically take place on three to six orders of magnitude longer time scales. For studies of intermittent, collisional interactions between biomolecules, particularly in membranes, the fluorescence lifetimes are thus often too short to allow diffusion-controlled

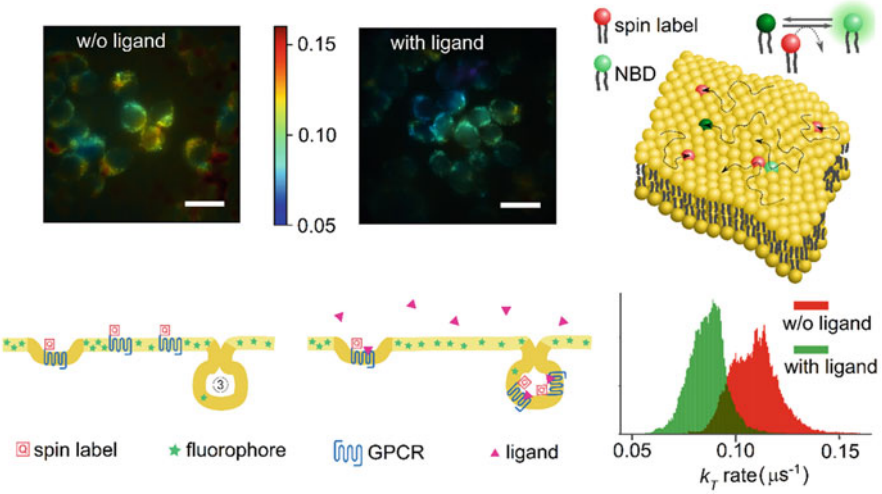

Fig. 6 TRAST imaging of low-frequency molecular encounters in membranes. Top right: Collisional encounters between fluorophore-labeled and spin-labeled molecules in a membrane can occur at time scales (μs to ms) which are much slower than the fluorescence lifetimes of most fluorophores (~ns). However, reversible singlet-triplet state transitions within the fluorophores (Fig. 1) can be readily affected. Left and middle: TRAST images of the triplet decay rate of NBD in the plasma membranes of 293T cells. The plasma membranes also contained spin marker (TEMPO) labeled GPCRs (NK1R). Upon binding of a ligand (SP), the GPCRs are internalized, and the spin labels are removed from the plasma membrane, which leads to a lower NBD triplet state decay rate, k_T, in the membrane. Bottom right: Cumulative histograms of k_T rates, as imaged by TRAST, with and without ligand added to the cells. See main text, and [40] for further details

collisional encounters with quenchers to significantly affect the fluorophore emission. Fluorescent probes with longer fluorescence lifetimes are rare, in particular if they both need to have a high fluorescence brightness and to be efficiently quenched by contact [52]. As a way to overcome these drawbacks, quenching of long-lived triplet states of fluorophores can be monitored via fluorescence, combining the sensitivity of fluorescence detection with the environmental sensitivity of the long-lived triplet and other dark transient states (Fig. 1). Based on this principle, we have shown in previous work how FCS measurements, monitoring fluorescence intensity fluctuations resulting from transitions between singlet and triplet states in membrane-bound fluorophores (Fig. 2), can be used to quantify quenching of the fluorophore triplet states by spin labels in the membranes [53]. Thereby, molecular encounters between the fluorophores and spin labels in the membranes can be monitored at ms^{-1} to μs^{-1} frequencies, at which practically no quenching of the fluorescence intensity occurs. More recently, based on the same principle, we introduced TRAST to follow the interaction between a spin-labeled G-protein coupled receptor (GPCR) (the neurokinin 1 receptor, NK1R) and lipids in the plasma membranes of live cells, labeled with the fluorophore NBD (7-nitrobenz-2-oxa-1,3-diazole-4-yl). NK1R is involved in several physiological and pathophysiological functions and is an important therapeutic target [54]. In its resting state, NK1R has been found to form clusters in the plasma membrane of 293T cells [55]. After activation with its natural ligand, substance P (SP), the receptor localization then changes significantly [56]. This reorganization is principally the result of the fast internalization of activated receptors. We found that the transient state kinetics of NBD labels in the plasma membranes differed significantly upon NK1R activation by its agonist SP. This reflects differences in the transient interactions between the GPCR and the labeled lipids, which could be attributed to modifications in the membrane environment upon activation. The observed changes could be monitored via the quenching rates, both on a whole-cell level, but also in a spatially resolved manner with sub-cellular resolution (Fig. 6, upper left and middle images).

From a more general perspective, GPCRs have a central role in transducing extracellular signals into intracellular responses and represent a majority of all drug targets. Lately, studies of GPCRs by, e.g., X-ray crystallography and cryo-EM have dramatically advanced the knowledge of structure-function relationships, but a complete understanding of GPCR function is impossible to attain without added information about GPCRs dynamics [2]. Here, GPCR–lipid interactions play an important role, but are often transient in character, and occur too intermittently to be readily observable by available technologies. By TRAST however, such protein–lipid interactions can be followed and imaged [40].

5 Concluding Remarks

Fluorophore dark state transitions are both a concern and a prerequisite for fluorescence-based SMD and SRM techniques, and considerable effort has been spent on investigating these phenomena. Yet, an additional aspect of fluorophore blinking has been largely overlooked, namely the strong environmental sensitivity and that fluorophore blinking properties thereby can provide additional fluorescence-based readout parameters. In this review, the principles of the TRAST technique are presented, and examples are given on how this technique can be applied to monitor and image different dark state transitions, reflecting microenvironmental conditions and molecular interactions not detectable via other fluorescence parameters. Alterations in such local cellular conditions, including local oxygen concentrations, redox conditions, and local fluidities, mobilities and molecular interactions, have been found to be both manifestations and driving forces behind several disease conditions, and thus of large biomedical relevance. It is therefore important to have adequate, widely applicable means to monitor such conditions, and here the TRAST approach can play an important role.

Acknowledgments The author likes to acknowledge the important contributions of present and past co-workers in the group, in the development and applications of the TRAST technique. This work was supported by funds from the Swedish Research Council (VR), the Knut and Alice Wallenberg Foundation (KAW), and the Swedish Foundation for Strategic Research (SSF).

References

1. Ehrenberg M (2014) Super-resolved fluorescence microscopy, scientific background on the Nobel prize in chemistry 2014. The Royal Swedish Academy of Sciences
2. Gusach A, Maslov I, Luginina A, Borshchevskiy V, Mishin A, Cherezov V (2020) Beyond structure: emerging approaches to study GPCR dynamics. Curr Opin Struct Biol 63:18–25
3. Jacobson K, Liu P, Lagerholm BC (2019) The lateral organization and mobility of plasma membrane components. Cell 177:806–819
4. Blom H, Widengren J (2017) Stimulated emission depletion microscopy. Chem Rev 117:7377–7427
5. Gupta A, Sankaran J, Wohland T (2019) Fluorescence correlation spectroscopy: the technique and its applications in soft matter. Phys Sci Rev 4. https://doi.org/10.1515/psr-2017-0104
6. Su D, Hou YM, Dong CQ, Ren JC (2019) Fluctuation correlation spectroscopy and its applications in homogeneous analysis. Anal Bioanal Chem 411:4523–4540
7. Schermelleh L, Ferrand A, Huser T, Eggeling C, Sauer M, Biehlmaier O, Drummen GPC (2019) Super-resolution microscopy demystified. Nat Cell Biol 21:72–84
8. Farka Z, Mickert MJ, Pastucha M, Mikusova Z, Skladal P, Gorris HH (2020) Advances in optical single-molecule detection: en route to supersensitive bioaffinity assays. Angew Chem Int Ed 59:10746–10773
9. Gwosch KC, Pape JK, Balzarotti F, Hoess P, Ellenberg J, Ries J, Hell SW (2020) MINFLUX nanoscopy delivers 3D multicolor nanometer resolution in cells. Nat Methods 17:217-+
10. Porter G (1950) Flash photolysis and spectroscopy. A new method for the study of free radical reactions. Proc R Soc A 200:284–300

11. Vanderkooi JM, Calhoun DB, Englander SW (1987) On the prevalence of room-temperatur protein phosphorescence. Science 236:568–569
12. Van Amerongen H, Van Grondelle R (1995) Transient absorption-spectroscopy in study of processes and dynamics in biology. Biochem Spectrosc 246:201–226
13. Lorenc M, Ziolek M, Naskrecki R, Karolczak J, Kubicki J, Maciejewski A (2002) Artifacts in femtosecond transient absorption spectroscopy. Appl Phys B Lasers Opt 74:19–27
14. Jovin TM, Vaz WLC (1989) Rotational and translational diffusion in membranes measured by fluorescence and phosphorescence methods. Methods Enzymol 172:471–513
15. Cioni P, Strambini GB (2002) Tryptophan phosphorescence and pressure effects on protein structure. BBA-Protein Struct M 1595:116–130
16. Yu Q, Huang TC, Li YP, Wei HJ, Liu SJ, Huang W, Du J, Zhao Q (2017) Rational design of a luminescent nanoprobe for hypoxia imaging in vivo via ratiometric and photoluminescence lifetime imaging microscopy. Chem Commun 53:4144–4147
17. Widengren J, Mets Ü (2001) Conceptual basis of fluorescence correlation spectroscopy and related techniques as tools in bioscience. In: Zander C, Enderlein J, Keller RA (eds) Single molecule detection in solution: methods and applications. Wiley-VCH, Heidelberg, pp 69–120
18. Rigler R, Mets U, Widengren J, Kask P (1993) Fluorescence correlation spectroscopy with high count rate and low-background - analysis of translational diffusion. Eur Biophys J Biophys Lett 22:169–175
19. Widengren J, Mets Ü, Rigler R (1995) Fluorescence correlation spectroscopy of triplet-states in solution - a theoretical and experimental-study. J Phys Chem 99:13368–13379
20. Widengren J, Dapprich J, Rigler R (1997) Fast interactions between Rh6G and dGTP in water studied by fluorescence correlation spectroscopy. Chem Phys 216:417–426
21. Widengren J, Schwille P (2000) Characterization of photoinduced isomerization and back-isomerization of the cyanine dye Cy5 by fluorescence correlation spectroscopy. J Phys Chem A 104:6416–6428
22. Widengren J, Seidel CAM (2000) Manipulation and characterization of photo-induced transient states of Merocyanine 540 by fluorescence correlation spectroscopy. Phys Chem Chem Phys 2: 3435–3441
23. Koppel DE (1974) Statistical accuracy in fluorescence correlation spectroscopy. Phys Rev A 10: 1938–1945
24. Sanden T, Persson G, Thyberg P, Blom H, Widengren J (2007) Monitoring kinetics of highly environment sensitive states of fluorescent molecules by modulated excitation and time-averaged fluorescence intensity recording. Anal Chem 79:3330–3341
25. Widengren J (2010) Fluorescence-based transient state monitoring for biomolecular spectroscopy and imaging. J R Soc Interface 7:1135–1144
26. Kimble HJ, Dagenais M, Mandel L (1977) Photon anti-bunching in resonance fluorescence. Phys Rev Lett 39:691–695
27. Ehrenberg M, Rigler R (1974) Rotational brownian-motion and fluorescence intensity fluctuations. Chem Phys 4:390–401
28. Kask P, Piksarv P, Mets U (1985) Fluorescence correlation spectroscopy in the nanosecond time range - photon antibunching in the dye fluorescence. Eur Biophys J Biophys Lett 12:163–166
29. Mets U, Widengren J, Rigler R (1997) Application of the antibunching in dye fluorescence: measuring the excitation rates in solution. Chem Phys 218:191–198
30. Hevekerl H, Tornmalm J, Widengren J (2016) Fluorescence-based characterization of non-fluorescent transient states of tryptophan - prospects for protein conformation and interaction studies. Sci Rep 6:35052
31. Sanden T, Persson G, Widengren J (2008) Transient state imaging for microenvironmental monitoring by laser scanning microscopy. Anal Chem 80:9589–9596
32. Tornmalm J, Widengren J (2018) Label-free monitoring of ambient oxygenation and redox conditions using the photodynamics of flavin compounds and transient state (TRAST) spectroscopy. Methods 140:178–187

33. Spielmann T, Xu L, Gad AKB, Johansson S, Widengren J (2014) Transient state microscopy probes patterns of altered oxygen consumption in cancer cells. FEBS J 281:1317–1332
34. Chmyrov V, Spielmann T, Hevekerl H, Widengren J (2015) Trans-Cis isomerization of lipophilic dyes probing membrane microviscosity in biological membranes and in live cells. Anal Chem 87:5690–5697
35. Geissbuehler M, Spielmann T, Formey A, Marki I, Leutenegger M, Hinz B, Johnsson K, Van De Ville D, Lasser T (2010) Triplet imaging of oxygen consumption during the contraction of a single smooth muscle cell (A7r5). Biophys J 98:339–349
36. Spielmann T, Blom H, Geissbuehler M, Lasser T, Widengren J (2010) Transient state monitoring by total internal reflection fluorescence microscopy. J Phys Chem B 114:4035–4046
37. Mucksch J, Spielmann T, Sisamakis E, Widengren J (2015) Transient state imaging of live cells using single plane illumination and arbitrary duty cycle excitation pulse trains. J Biophotonics 8:392–400
38. Karampatzakis A, Sankaran J, Kandaswamy K, Rice SA, Cohen Y, Wohland T (2017) Measurement of oxygen concentrations in bacterial biofilms using transient state monitoring by single plane illumination microscopy. Biomed Phys Eng Express 3:035020
39. Tornmalm J, Sandberg E, Rabasovic M, Widengren J (2019) Local redox conditions in cells imaged via non-fluorescent transient states of NAD(P)H. Sci Rep 9:15070
40. Tornmalm J, Piguet J, Chmyrov V, Widengren J (2019) Imaging of intermittent lipid-receptor interactions reflects changes in live cell membranes upon agonist-receptor binding. Sci Rep 9: 18133
41. Cairns RA, Harris IS, Mak TW (2011) Regulation of cancer cell metabolism. Nat Rev Cancer 11:85–95
42. Heiden MGV, Cantley LC, Thompson CB (2009) Understanding the Warburg effect: the metabolic requirements of cell proliferation. Science 324:1029–1033
43. Kroemer G, Pouyssegur J (2008) Tumor cell metabolism: Cancer's Achilles' heel. Cancer Cell 13:472–482
44. Seyfried TN, Shelton LM (2010) Cancer as a metabolic disease. Nutr Metab 7:7
45. Ward PS, Thompson CB (2012) Metabolic reprogramming: a cancer Hallmark even Warburg did not anticipate. Cancer Cell 21:297–308
46. Pace NA, Hennelly SP, Goodwin PM (2021) Immobilization of cyanines in DNA produces systematic increases in fluorescence intensity. J Phys Chem Lett 12:8963–8971
47. Rashid F, Raducanu VS, Zaher MS, Tehseen M, Habuchi S, Hamdan SM (2019) Initial state of DNA-dye complex sets the stage for protein induced fluorescence modulation. Nat Commun 10:2104
48. Chmyrov A, Sanden T, Widengren J (2010) Iodide as a fluorescence quencher and promoter-mechanisms and possible implications. J Phys Chem B 114:11282–11291
49. Widengren J, Chmyrov A, Eggeling C, Lofdahl PA, Seidel CAM (2007) Strategies to improve photostabilities in ultrasensitive fluorescence spectroscopy. J Phys Chem A 111:429–440
50. Hanahan D, Weinberg RA (2011) Hallmarks of cancer: the next generation. Cell 144:646–674
51. Lakowicz JR (2006) Principles of fluorescence spectroscopy. Springer, New York
52. Melo E, Martins J (2006) Kinetics of bimolecular reactions in model bilayers and biological membranes. A critical review. Biophys Chem 123:77–94
53. Stromqvist J, Chmyrov A, Johansson S, Andersson A, Maler L, Widengren J (2010) Quenching of triplet state fluorophores for studying diffusion-mediated reactions in lipid membranes. Biophys J 99:3821–3830
54. Garcia-Recio S, Gascon P (2015) Biological and pharmacological aspects of the NK1-receptor. Biomed Res Int 2015:495704
55. Meyer BH, Segura JM, Martinez KL, Hovius R, George N, Johnsson K, Vogel H (2006) FRET imaging reveals that functional neurokinin-1 receptors are monomeric and reside in membrane microdomains of live cells. Proc Natl Acad Sci U S A 103:2138–2143

56. Veya L, Piguet J, Vogel H (2015) Single molecule imaging deciphers the relation between mobility and signaling of a prototypical G protein-coupled receptor in living cells. J Biol Chem 290:27723–27735